LDPC-Coded Index-Modulation Aided OFDM for In-vehicle Power Line Communications

Hongming Zhang, Lie-Liang Yang and Lajos Hanzo
School of ECS, University of Southampton, SO17 1BJ, UK.
Email: {zh1g11, lly, lh} @ecs.soton.ac.uk; http://www-mobile.ecs.soton.ac.uk.

***Abstract*—The recently developed orthogonal frequency-division multiplexing relying on index modulation (OFDM-IM) is adopted to the in-vehicle power line communications (PLCs) in order to combat the deleterious effects of frequency-selective fading and impulsive noise, whilst improving the energy efficiency of data communications. Furthermore, the low density parity check (LDPC) coding is invoked to further enhance the reliability of in-vehicle PLCs, which is of particular importance in light-weight airborne vehicles. For aiding LDPC decoding, a reduced complexity soft-decision detection scheme is proposed. The performance of the LDPC-coded OFDM-IM system is studied by simulation, when assuming communications over in-vehicle PLC channels. Our studies show that LDPC-coded OFDM-IM is capable of combating frequency-selective fading, mitigating impulsive noise, as well as striking a compelling trade-off between the spectral efficiency and energy efficiency for in-vehicle PLCs.**

I. Introduction

In-vehicle power line communication (PLC), which plays a significant role in intelligent light-weight airborne vehicles, has recently attracted considerable attentions. Information transmission in airborne vehicles can be implemented by using twisted wires or optical cables, both of which constitute a reliable communication medium. However, they both increase the weight, as well as the wiring harness complexity and cost of maintenance [1]. With the aid of the communications techniques recently developed for PLC systems, in-vehicle PLCs have became an attractive solution for circumventing the above-mentioned issues.

However, there are still further challenges. Firstly, when the electrical supply networks of vehicles are also used for data transmissions, they constitute a hostile propagation environment for communications. As shown in [1, 2], the in-vehicle PLC channels experience slowly time variant frequency-selective fading, which are additionally corrupted by impulsive noise. In detail, the time variation of in-vehicle PLC channels is usually caused by changes in the operating conditions of the vehicle. Furthermore, due to the multipath propagation phenomenon of the in-vehicle power line networks, as detailed in [3], a transmitted symbol may be spread over several adjacent symbols, hence, generating inter-symbol interference (ISI). Additionally, according to [4], the coherence bandwidth of in-vehicle PLC channels is between 500 kHz and 1.5 MHz, which is much lower than the total bandwidth required for satisfying all the communications, requirements quantitatively, the latter may be up to 100 MHz. Therefore, the in-vehicle PLC channels are typically frequency-selective. Finally, there is also substantial impulsive noise in in-vehicle PLCs, which is generated by the ignition as well as other switching events of the electrical equipment connected to the power line network. Although the above-mentioned characteristics are similar to those of the indoor PLC channels, the existing indoor PLC systems cannot be directly invoked for in-vehicle PLCs. Firstly, these two types of PLC systems have different dimensions' impairment and different types of wire topologies. Secondly, airborne in-vehicle PLC systems are usually energy limited, whilst indoor PLC systems are usually not. Thus, when considering all the above-mentioned issues, the PLC systems designed for vehicles should be able to combat frequency-selective fading and impulsive noise, as well as support energy-efficient operation.

In PLC, orthogonal frequency-division multiplexing (OFDM) can be employed for combatting the frequency-selective fading [5, 6]. Based on the classic OFDM concepts relying on index modulation (OFDM-IM) [7–9] has also been proposed for wireless communications. Owing to the introduction of the IM component, it has been shown in [7–9] that OFDM-IM is capable of striking an attractive tradeoff between the spectral efficiency and energy efficiency.

Therefore, in this paper, we extend the OFDM-IM concept to in-vehicle PLC. Specifically, we propose an low density parity check (LDPC) coded OFDM-IM system, in order to combat the frequency-selective fading as well as for mitigating the effects of impulsive noise. For the sake of achieving low-complexity LDPC decoding, we propose a novel technique of generating the soft information of the specific data bits implicitly conveyed by the active/passive subcarrier indices and by the classic amplitude-phase modulation (APM) symbols. Finally, the performance of our LDPC-coded OFDM-IM system is studied by simulations, when communicating over the in-vehicle PLC channels characterized by the measurements of [2, 10]. Our studies suggest that OFDM-IM constitutes a promising in-vehicle PLC scheme, which can be designed to strike a compelling tradeoff between the attainable data rate and energy efficiency.

The rest of the paper is organized as follows. In Section II, both the system model and in-vehicle PLC channels are detailed. Section III introduces the soft-decision detection and decoding scheme. Then, the achievable system performance is studied by simulation in Section IV. Finally, we offer our conclusions in Section V.

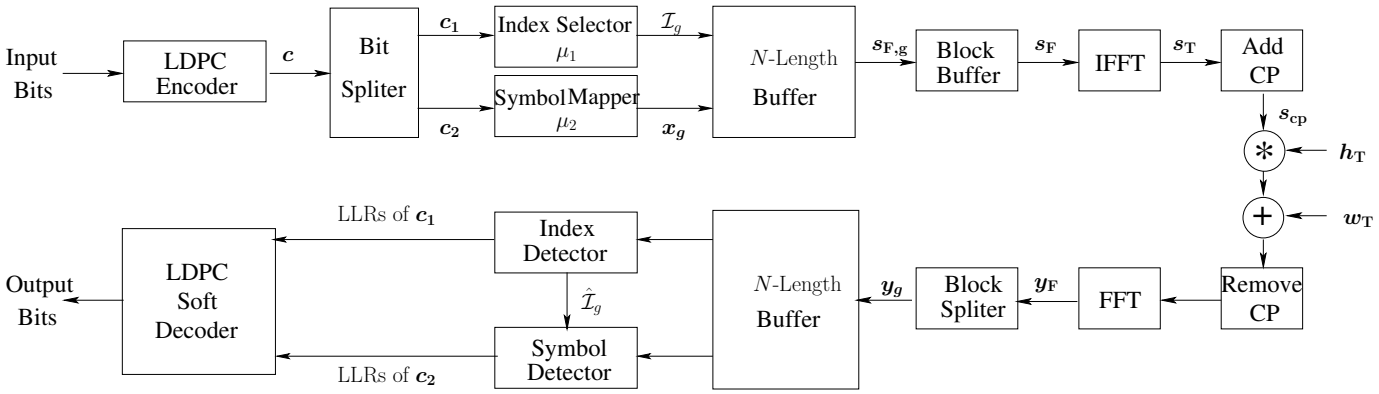

Fig. 1: Illustration of the LDPC-coded OFDM-IM system

II. System Model

A. Transmitter

We consider the LDPC-coded OFDM-IM system illustrated in Fig. 1. During a transmission block, a sequence of i.i.d. information bits denoted as $\boldsymbol{b} \in \{0,1\}^{RJ}$ is encoded by an R-rate LDPC encoder $\mathcal{C}$, yielding the coded bits $\boldsymbol{c} \in \{0,1\}^{J}$. Then, the coded bits in $\boldsymbol{c}$ are split into two sequences, where the first sequence denoted as $\boldsymbol{c}_1$ is used for index selection, while the second sequence denoted as $\boldsymbol{c}_2$ is used for APM, such as PSK or QAM. As seen in Fig. 1, the coded bits in $\boldsymbol{c}_1$ are first mapped into index symbols according to an index mapper μ_1: $\{0,1\}^{L_1} \to \mathcal{Z}$, where $\mathcal{Z} = \{\mathcal{Z}_1, \ldots, \mathcal{Z}_C\}$ contains $C = 2^{L_1}$ index subsets, each of which is formed with K indices chosen from N available indices, as shown in [9]. Thereby, we have $L_1 = \log_2 C = \left\lfloor \log_2 \binom{N}{K} \right\rfloor$. Let the cth index subset of $\mathcal{Z}$ be denoted as $\mathcal{Z}_c = \{\mathcal{Z}_c(0), \ldots, \mathcal{Z}_c(K-1)\} \subset \mathcal{Z}$, where $\mathcal{Z}_c(k) \in \mathbb{Z}_+^N$ for $k = 0, \ldots, K-1$. Assume that the gth group of data bits is mapped into the cth candidate in $\mathcal{Z}$. Then, for the sake of presentation, let the gth group of the index symbol be denoted as $\mathcal{I}_g = \mathcal{Z}_c \subset \mathcal{Z}$. On the other hand, the coded bits in $\boldsymbol{c}_2$ are mapped onto APM symbols according to a mapping μ_2: $\{0,1\}^{L_2} \to \mathcal{A}$, where $\mathcal{A}$ denotes the alphabet of a Q-ary constellation, where we have $Q = |\mathcal{A}|$ and hence $L_2 = \log_2(Q)$. Let us denote the K APM symbols transmitted by the indices of the gth group as $\boldsymbol{x}_g = [x_g(0), \ldots, x_g(K-1)]^T$ for $g = 0, 1, \ldots, G-1$, where we assume that $\mathbb{E}[|x_g(k)|^2] = 1$, $\forall x_g(k) \in \mathcal{A}$. As shown in Fig. 1, these APM symbols in $\boldsymbol{x}_g$ are transmitted by the active subcarriers having the indices in the set $\mathcal{I}_g$, yielding a block of the frequency-domain (FD) symbols $\boldsymbol{s}_{\mathrm{F},g} = [s_{\mathrm{F},g}(0), s_{\mathrm{F},g}(1), \ldots, s_{\mathrm{F},g}(N-1)]^T$, which can be expressed as

$$\boldsymbol{s}_{\mathrm{F},g} = \boldsymbol{I}_g \boldsymbol{x}_g, \tag{1}$$

where $\boldsymbol{I}_g$ is a mapping matrix whose columns are extracted from an $(N \times N)$-element identity matrix according to the indices in the set $\mathcal{I}_g$. Collecting the symbols transmitted by the G groups of indices, the FD symbols can be formulated as $\boldsymbol{s}_{\mathrm{F}} = \left[\boldsymbol{s}_{\mathrm{F},0}^T, \boldsymbol{s}_{\mathrm{F},1}^T, \ldots, \boldsymbol{s}_{\mathrm{F},G-1}^T\right]^T$, which are input to the M-point IFFT, yielding the time-domain (TD) symbols $\boldsymbol{s}_{\mathrm{T}} = \sqrt{\rho}\boldsymbol{\mathcal{F}}_M^H \boldsymbol{s}_{\mathrm{F}}$, where $\rho = M/(kG)$ is employed to normalize $\mathbb{E}[\|\boldsymbol{s}_{\mathrm{T}}\|_2^2] = 1$. Hence, we can readily show that the number of information bits conveyed by each subcarrier is $L_s = R\left(\left\lfloor \log_2 \binom{N}{K} \right\rfloor + K \log_2 Q\right)/N$, where we have $M = NG$. Finally, after concatenating a cyclic prefix (CP) of length L_{cp}, the baseband symbols expressed as $\boldsymbol{s}_{\mathrm{cp}} = \boldsymbol{I}_{\mathrm{CP}}^T \boldsymbol{s}_{\mathrm{T}}$, where $\boldsymbol{I}_{\mathrm{CP}} = [\boldsymbol{I}_{\mathrm{cp}}, \boldsymbol{I}_M]$ and $\boldsymbol{I}_{\mathrm{cp}}$ is a $(M \times L_{\mathrm{cp}})$ mapping matrix obtained from the last L_{cp} columns of an identity matrix $\boldsymbol{I}_M$, are transmitted over the in-vehicle power line channels characterized below.

B. In-vehicle Power Line Communication Channel

Due to the activity of the various electrical equipment connected to the power line, in-vehicle PLC channels exhibit a time-variant frequency-selective channel transfer function (CTF). Typically, the coherence time of in-vehicle power line channels is much higher than an OFDM symbol duration. Thus, we can usually assume that the channels remain constant during transmission of a single OFDM symbol. Moreover, we can assume that the sub-channel bandwidth satisfies $B_{\mathrm{s}} < B_{\mathrm{c}}$, where B_{c} denotes the channel's coherence bandwidth. Specifically, in this paper, the measurement based channel model of [10] is employed, which has the CTF of

$$h_{\mathrm{F}}(f) = \frac{S_{21}(f)}{2}, \tag{2}$$

where $S_{21}(f)$ is the forward transfer function as detailed in [4, 10], which can be measured using a vectorial network analyzer (VNA). Specifically, when the OFDM signals of Section I are transmitted over the in-vehicle PLC channels, the discrete-time baseband equivalent FD channel transfer factor (FDCHTF) of the mth subchannel is defined as $h_{\mathrm{F}}(m) \triangleq h_{\mathrm{F}}(f = m\Delta f)$, where Δf is the frequency spacing between the adjacent sub-bands.

The in-vehicle power line noise is constituted by the superposition of the background noise and impulsive noise, where the background noise is always present, while the impulsive noise only occurring from time to time. As shown in [11], the TD impulsive noise can be characterized by its duration time t_1, inter-arrival time t_0 and power. This also means

that during the inter-arrival time t_0, there is only background noise, while during the time t_1, both background noise and impulsive noise are encountered. As for the background noise, it was stated in [11] that in the frequency band spanning from 500 kHz to 2 MHz, the power spectral density (PSD) ramps down from -110 dBm/Hz to -130 dBm/Hz, and then remains constant beyond 2 MHz. For the time-invariant in-vehicle PLC channels, we assume that the PSD of the background noise is also time-invariant. Hence, we can model the in-vehicle background noise as colored Gaussian noise with its instantaneous PSD denoted as $N_{w_1}(f)$, where for the mth subchannel, we have $N_{w_1}(m) \triangleq N_{w_1}(f = m\Delta f)$. By contrast, for the FD impulsive noise, we define the ratio between the impulsive noise power and background noise power as Λ_{Po}, which is assumed to be a constant value for our study. Note that as shown in [2, 12], impulsive noise usually appears with a higher instantaneous PSD in the lower frequency band. Thus, without loss of generality, we may assume that the impulsive noise occurs only in the frequency band below f_{TS}.

Based on the above characteristics of the in-vehicle power line noise, the noise samples of the mth subchannel may be written as

$$w_{\text{F}}(m) = w_0(m) + \eta_{m,t} w_1(m), \tag{3}$$

where $\eta_{m,t} \in \{0, 1\}$ is the occurrence indicator of impulsive noise, which is dependent on both the duration time t_1 and the inter-arrival time t_0. Correspondingly, the PSD of the in-vehicle power line noise imposed on the mth subchannel can be expressed as

$$N_w(m) = \begin{cases} \Lambda_{\text{Po}} N_{w_0}(m) & \text{for } \eta_{m,t} = 1 \text{ and } f \leq f_{\text{TS}} \\ N_{w_0}(m) & \text{otherwise} \end{cases}. \tag{4}$$

In this paper, we assume that the FD noise samples remain are statistically independent amongst the subchannels after receiver filtering. Hence, the FD noise samples can be assumed to obey the multivariate Gaussian distribution with a mean of zeros and a covariance matrix of $\mathbf{\Sigma} = \text{diag}\{\sigma_w^2(0), \sigma_w^2(1), \ldots, \sigma_w^2(M-1)\}$, where by definition we have $\sigma_w^2(m) = N_w(m)\Delta f$.

C. Received Signals

Let us assume that $L_{\text{cp}} \geq L_{\text{h}}$ and that perfect synchronization is achieved at the receiver. As shown in Fig. 1, after removing the CP and carrying out the FFT, the FD received baseband equivalent observations $\boldsymbol{y}_{\text{F}} = [y_{\text{F}}(0), y_{\text{F}}(1), \ldots, y_{\text{F}}(M-1)]^T$ can be formulated as

$$\boldsymbol{y}_{\text{F}} = \sqrt{\rho}\boldsymbol{H}\boldsymbol{s}_{\text{F}} + \boldsymbol{w}_{\text{F}}, \tag{5}$$

where $\boldsymbol{H} = \text{diag}\{h_{\text{F}}(0), h_{\text{F}}(1), \ldots, h_{\text{F}}(M-1)\}$ and $h_{\text{F}}(m)$ is given in Section II-B. In (5), $\boldsymbol{w}_{\text{F}}$ contains the background noise and the potential impulsive noise, as argued in Section II-B. Then, the received FD symbols in $\boldsymbol{y}_{\text{F}}$ are sent to a detector, as detailed in the next section.

III. Data Detection and Decoding

In this section, we consider the soft-decision detection of both the index symbols and APM symbols, so as to provide soft inputs to the soft LDPC decoder. In the rest of this section, we assume that perfect channel estimation and noise state estimation are accomplished at the receiver, i.e. the elements in $\boldsymbol{H}$ and $\mathbf{\Sigma}$ are perfectly known. Then, with the aid of (1) and (5), for the gth group symbols, we have

$$\boldsymbol{y}_g = \sqrt{\rho}\boldsymbol{H}_g\boldsymbol{I}_g\boldsymbol{x}_g + \boldsymbol{w}_g, \tag{6}$$

where $\boldsymbol{H}_g$ and $\boldsymbol{w}_g$ contain elements of the gth group from $\boldsymbol{H}$ and $\boldsymbol{w}_{\text{F}}$, respectively. Then, the conditional probability density function (PDF) of $\boldsymbol{y}_g$ can be expressed as

$$p\left(\boldsymbol{y}_g|\mathcal{I}_g, \boldsymbol{x}_g\right) = \frac{1}{\pi^N \mathbf{\Sigma}_g} \exp\left\{-\Phi(\mathcal{I}_g, \boldsymbol{x}_g)\right\}, \tag{7}$$

where for the sake of presentation, we define

$$\mathbf{\Phi}(\mathcal{I}_g, \boldsymbol{x}_g) \triangleq \left(\boldsymbol{y}_g - \sqrt{\rho}\boldsymbol{H}_g\boldsymbol{I}_g\boldsymbol{x}_g\right)^H \mathbf{\Sigma}_g^{-1} \left(\boldsymbol{y}_g - \sqrt{\rho}\boldsymbol{H}_g\boldsymbol{I}_g\boldsymbol{x}_g\right), \tag{8}$$

where $\sqrt{\rho}\boldsymbol{H}_g\boldsymbol{I}_g\boldsymbol{x}_g$ and $\mathbf{\Sigma}_g$ are the mean vector and the covariance matrix of $\boldsymbol{y}_g$, respectively.

In order to carry out soft LDPC decoding, soft estimation of the coded bits in $\boldsymbol{c}_{1,g}$ and $\boldsymbol{c}_{2,g}$ is required. Let us first derive the soft information for the coded bits in $\boldsymbol{c}_{1,g}$. Stipulating the idealized simplifying assumption of having perfect channel state information (CSI), the maximum a posteriori (MAP) estimation of the lth coded bit $c_{1,g}(l)$ is obtained by computing the log-likelihood ratio (LLR) of

$$\lambda\left(c_{1,g}(l)|\boldsymbol{y}_g\right) = \ln \frac{p\left(c_{1,g}(l) = 1|\boldsymbol{y}_g\right)}{p\left(c_{1,g}(l) = 0|\boldsymbol{y}_g\right)}. \tag{9}$$

Let us assume that the a priori probability of the coded bit $c_{1,g}(l)$ is the same for all the coded bits. Then, according to [13], we have

$$\begin{aligned} \lambda\left(c_{1,g}(l)|\boldsymbol{y}_g\right) &= \ln \frac{\sum\limits_{\mathcal{Z}_{\alpha,1} \in \mathcal{Z}} p\left(\boldsymbol{y}_g|\mathcal{Z}_{\alpha,1}\right)}{\sum\limits_{\mathcal{Z}_{\alpha,0} \in \mathcal{Z}} p\left(\boldsymbol{y}_g|\mathcal{Z}_{\alpha,0}\right)} \\ &= \ln \frac{\sum\limits_{\mathcal{Z}_{\alpha,1} \in \mathcal{Z}} \sum\limits_{\boldsymbol{a}_\beta \in \mathcal{A}^K} p\left(\boldsymbol{y}_g|\mathcal{Z}_{\alpha,1}, \boldsymbol{a}_\beta\right)}{\sum\limits_{\mathcal{Z}_{\alpha,0} \in \mathcal{Z}} \sum\limits_{\boldsymbol{a}_\beta \in \mathcal{A}^K} p\left(\boldsymbol{y}_g|\mathcal{Z}_{\alpha,0}, \boldsymbol{a}_\beta\right)}, \end{aligned} \tag{10}$$

where $\mathcal{Z}_{\alpha,0}$ and $\mathcal{Z}_{\alpha,1}$ are the subsets of $\mathcal{Z}$ given as $\mathcal{Z}_{\alpha,0} \triangleq \{\mathcal{Z}_\alpha \in \mathcal{Z} : c_{1,g}(l) = 0\}$ and likewise, $\mathcal{Z}_{\alpha,1} \triangleq \{\mathcal{Z}_\alpha \in \mathcal{Z} : c_{1,g}(l) = 1\}$. Upon substituting (7) into (10), we arrive at

$$\lambda\left(c_{1,g}(l)|\boldsymbol{y}_g\right) = \ln \frac{\sum\limits_{\mathcal{Z}_{\alpha,1} \in \mathcal{Z}} \sum\limits_{\boldsymbol{a}_\beta \in \mathcal{A}^K} \exp\left\{-\mathbf{\Phi}(\mathcal{Z}_{\alpha,1}, \boldsymbol{a}_\beta)\right\}}{\sum\limits_{\mathcal{Z}_{\alpha,0} \in \mathcal{Z}} \sum\limits_{\boldsymbol{a}_\beta \in \mathcal{A}^K} \exp\left\{-\mathbf{\Phi}(\mathcal{Z}_{\alpha,0}, \boldsymbol{a}_\beta)\right\}}. \tag{11}$$

In order to avoid numerical overflow, the Jacobian logarithm [14] can be applied recursively for computing (11), yielding

$$\begin{aligned}\lambda\left(c_{1,g}(l)|\boldsymbol{y}_g\right) \approx & J_{\mathcal{Z}_{\alpha,1}\in\mathcal{Z}}\left\{J_{\boldsymbol{a}_\beta\in\mathcal{A}^K}\left\{-\boldsymbol{\Phi}(\mathcal{Z}_{\alpha,1},\boldsymbol{a}_\beta)\right\}\right\} \\ & - J_{\mathcal{Z}_{\alpha,0}\in\mathcal{Z}}\left\{J_{\boldsymbol{a}_\beta\in\mathcal{A}^K}\left\{-\boldsymbol{\Phi}(\mathcal{Z}_{\alpha,0},\boldsymbol{a}_\beta)\right\}\right\},\end{aligned} \tag{12}$$

where $J\{\cdot\}$ denotes a recursive function of the Jacobian logarithm, as detailed in [14].

For the the coded bit $c_{2,g}(l)$ in $\boldsymbol{c}_{2,g}$, the same detection process can be carried out as detailed above in order to obtain its LLR, which is denoted as $\lambda\left(c_{2,g}(l)|\boldsymbol{y}_g\right)$. However, in order to reduce the computational complexity, a sub-optimal detection process is introduced, which is detailed as follows. Firstly, similar to (9) and (10), we have

$$\lambda\left(c_{2,g}(l)|\boldsymbol{y}_g\right) = \ln \frac{\sum\limits_{\boldsymbol{a}_{\beta,1}\in\mathcal{A}^K}\sum\limits_{\mathcal{Z}_\alpha\in\mathcal{Z}} p\left(\boldsymbol{y}_g|\mathcal{Z}_\alpha,\boldsymbol{a}_{\beta,1}\right)}{\sum\limits_{\boldsymbol{a}_{\beta,0}\in\mathcal{A}^K}\sum\limits_{\mathcal{Z}_\alpha\in\mathcal{Z}} p\left(\boldsymbol{y}_g|\mathcal{Z}_\alpha,\boldsymbol{a}_{\beta,0}\right)}, \tag{13}$$

where $\boldsymbol{a}_{\beta,0}$ and $\boldsymbol{a}_{\beta,1}$ are the subsets of $\mathcal{A}^K$, given by $\boldsymbol{a}_{\beta,0} \triangleq \{\boldsymbol{a}_\beta \in \mathcal{A}^K : c_{2,g}(l) = 0\}$ and $\boldsymbol{a}_{\beta,1} \triangleq \{\boldsymbol{a}_\beta \in \mathcal{A}^K : c_{2,g}(l) = 1\}$, respectively. However, instead of considering all the index candidates in the set $\mathcal{Z}$ for calculating the LLR $\lambda\left(c_{2,g}(l)|\boldsymbol{y}_g\right)$, the detected results of the coded bits in $\boldsymbol{c}_{1,g}$ can be used for reducing the computational complexity at this stage. In detail, hard-decisions based on the LLRs of $\boldsymbol{c}_{1,g}$ can be first made to obtain the index symbols $\hat{\mathcal{I}}_g$. Then, the LLR for $c_{2,g}(l)$ can be formulated as

$$\begin{aligned}\lambda_{\text{sub}}\left(c_{2,g}(l)|y_g(i)\right) = & \ln \frac{\sum\limits_{a_{\beta,1}\in\mathcal{A}} p\left(y_g(i)|i=\hat{\mathcal{I}}_g(k),a_{\beta,1}\right)}{\sum\limits_{a_{\beta,0}\in\mathcal{A}} p\left(y_g(i)|i=\hat{\mathcal{I}}_g(k),a_{\beta,0}\right)} \\ \approx & J_{a_{\beta,1}\in\mathcal{A}}\left\{-\Phi(i,a_{\beta,1})\right\} \\ & - J_{a_{\beta,0}\in\mathcal{A}}\left\{-\Phi(i,a_{\beta,0})\right\}.\end{aligned} \tag{14}$$

Upon comparing (13) with (14), we can readily show that the computational complexity of (14) is significantly lower than that of (13).

Finally, the J-length LLRs for the coded bits in $\boldsymbol{c}$ are forwarded to the soft LDPC decoder, which provides the final decoded bits. Specifically, in this paper, the sum-product algorithm (SPA) based decoder is assumed for LDPC decoding, while the details of the SPA decoder adopted for LDPC codes can be found in [15].

IV. Performance Results

In this section, the attainable system performance is studied using simulations, where an irregular LDPC code having a rate of $R = 1/2$ and a codeword length of $J = 5000$ are employed. Moreover, the SPA decoder with a maximum of 50 iterations is used. We focus our attention on the case of $M = 256$ subcarriers using QPSK modulation, operating in the 2-76.8 MHz frequency range. For modelling the in-vehicle PLC channels, the measurement results of [10] are relied upon. Specifically, in our simulations the direct link between the right front light and left front light of the 2006 Pontiac Solstice is used. It has a coherence bandwidth of $B_c = 1.09$ MHz and a maximum delay spread of 0.8 μs. Thus, the CP length in our system is chosen to be $L_{\text{cp}} = 70$. For characterizing the background noise and impulsive noise, the measurement results of [2] are employed. In detail, the PSD of the background noise is chosen to be $N_{w_0}(m) = -115$ dBm/kHz, while the ratio between impulsive noise power and background noise power is set to $\Lambda_{\text{Po}} = 35$ dB. Moreover, the frequency band of the impulsive noise is chosen to be $f_{\text{TS}} = 25$ MHz. The inter-arrival time of impulsive noise is chosen to be $t_0 = 30$ ms, while the duration time is set be $t_1 = 10$ μs. Throughout this section, the SNR is the ratio between the transmitted power of an OFDM symbol and the power of the background noise.

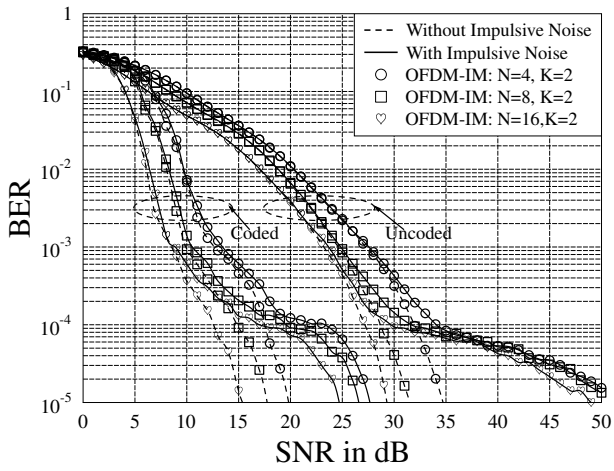

Fig. 2: BER performance of the LDPC-coded OFDM-IM system using QPSK, when communicating over the dispersive in-vehicle PLC channel contaminated by both background noise and impulsive noise.

In Fig. 2 and Fig. 3, we investigate the BER performance of the LDPC-coded OFDM-IM system relying on QPSK, when communicating over the in-vehicle PLC channels contaminated by both background noise and impulsive noise. In Fig. 2, each group of OFDM-IM symbols chooses $K = 2$ activated indices from a total of $N = 4, 8$, or 16 available indices, yielding a total of $L_s = 0.75$, 0.5, or 0.3125 transmitted information bits per subcarrier. While, in Fig. 3, each group of OFDM-IM symbols chooses $K = 1, 2$, or 3 activated indices from a total of $N = 16$ available indices, yielding a total of $L_s = 0.1875$, 0.3125, or 0.4688 transmitted information bits per subcarrier. From the results of Fig. 2 and Fig. 3, we have the following observations. Firstly, when the LDPC code is not used and impulsive noise doesn't occurs, the BER performance of the system improves, as L_s decreases. This general observation is also valid for the uncoded OFDM-IM system in wireless communications. However, when impulsive noise occurs, error floors appear in the high SNR region of the uncoded systems. This is because in the high SNR region,

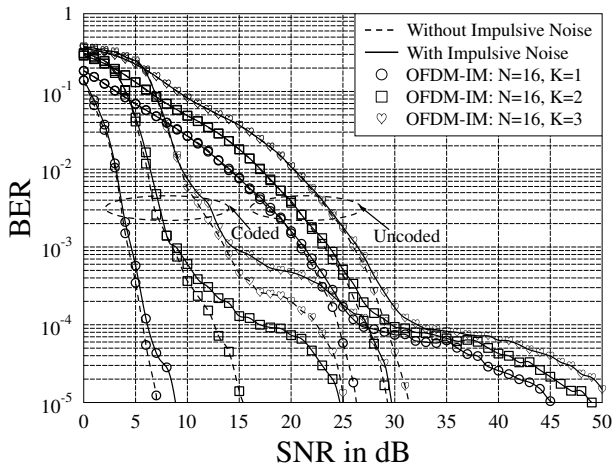

Fig. 3: BER performance of the LDPC-coded OFDM-IM system using QPSK, when communicating over the dispersive in-vehicle PLC channel contaminated by both background noise and impulsive noise.

the impulsive noise dominates the detection performance of the system. In the OFDM-IM systems, the impulsive noise having a high instantaneous power may mislead the detection of the activated indices. As a result, the system performance is severely degraded. Secondly, as seen in Fig. 2, when the LDPC code is employed, despite the occurrence of impulsive noise, the BER performance of the OFDM-IM system is improved, when L_s is decreased. Furthermore, we observe a gradual slope change for the BER curve at a certain value of BER. This observation can be explained with the aid of the specific detection scheme shown in Section III. As shown in (14), the sub-optimal LLRs of the coded bits in $\boldsymbol{c}_2$ are calculated based on the hard decision of index symbols. Thus, an incorrect detection of the index symbol usually results in an incorrect detection of the APM symbols. As a result, the BER performance of the decoder is severely degraded, especially in the presence of impulsive noise. Furthermore, as shown in Fig. 3, when the value of N is fixed, the BER performance of the OFDM-IM system decreases as the value of K increases. This is because that as the number of active indices increases, the probability of incorrect detections of index symbols increases, which may further degrade the detection performance of the APM symbols. Hence, as the value of K increases, the slope change of the BER curve becomes more gradually. Therefore, there exists a tradeoff between the detection complexity and the attainable system performance.

V. Conclusions

In this paper, an LDPC-coded OFDM-IM system has been designed for in-vehicle PLCs, in order to combat the associated frequency-selective fading, to mitigate the impulsive noise, as well as to achieves energy efficiency. Moreover, we have introduced a low-complexity soft-decision detection scheme for the LDPC-coded OFDM-IM system. The performance of the LDPC-coded OFDM-IM has been studied and compared to the relevant benchmark schemes, when assuming communications over the in-vehicle PLC channels experiencing both background noise and impulsive noise. Our studies demonstrated that the LDPC-coded OFDM-IM system constitutes a promising scheme for the in-vehicle PLCs.

References

[1] P. Degauque, I. Stievano, S. Pignari, V. Degardin, F. Canavero, F. Grassi, and F. Canete, "Power-line communication: Channel characterization and modeling for transportation systems," *IEEE Vehicular Technology Magazine*, vol. 10, no. 2, pp. 28–37, June 2015.

[2] A. B. Vallejo-Mora, J. J. Sanchez-Martinez, F. J. Canete, J. A. Cortes, and L. Diez, "Characterization and evaluation of in-vehicle power line channels," in *2010 IEEE Global Telecommunications Conference (GLOBECOM 2010)*, Dec 2010, pp. 1–5.

[3] I. Stievano, F. Canavero, W. G. Valverde, L. Guerrieri, and P. Bisaglia, "Multipath modeling of automotive power line communication channels," *IEEE Transactions on Industrial Informatics*, vol. 10, no. 2, pp. 1381–1391, May 2014.

[4] M. Lienard, M. Carrion, V. Degardin, and P. Degauque, "Modeling and analysis of in-vehicle power line communication channels," *IEEE Transactions on Vehicular Technology*, vol. 57, no. 2, pp. 670–679, March 2008.

[5] L. Hanzo, M. Münster, B. Choi, and T. Keller, *OFDM and MC-CDMA for Broadband Multi-user Communications, WLANs and Broadcasting*. John Wiley & Sons, May 2003.

[6] Lie-Liang Yang, *Multicarrier Communications*. John Wiley & Sons, Ltd, 2009.

[7] R. Abu-alhiga and H. Haas, "Subcarrier-index modulation OFDM," in *2009 IEEE 20th International Symposium on Personal, Indoor and Mobile Radio Communications*, Sept 2009, pp. 177–181.

[8] D. Tsonev, S. Sinanovic, and H. Haas, "Enhanced subcarrier index modulation (SIM) OFDM," in *2011 IEEE GLOBECOM Workshops (GC Wkshps)*, Dec 2011, pp. 728–732.

[9] E. Basar, U. Aygolu, E. Panayirci, and H. Poor, "Orthogonal frequency division multiplexing with index modulation," *IEEE Transactions on Signal Processing*, vol. 61, no. 22, pp. 5536–5549, Nov 2013.

[10] M. Mohammadi, L. Lampe, M. Lok, S. Mirabbasi, M. Mirvakili, R. Rosales, and P. van Veen, "Measurement study and transmission for in-vehicle power line communication," in *IEEE International Symposium on Power Line Communications and Its Applications (ISPLC), 2009*, March 2009, pp. 73–78.

[11] V. Degardin, M. Lienard, P. Degauque, E. Simon, and P. Laly, "Impulsive noise characterization of in-vehicle power line," *IEEE Transactions on Electromagnetic Compatibility*, vol. 50, no. 4, pp. 861–868, Nov 2008.

[12] M. Antoniali, M. D. Piante, and A. Tonello, "PLC noise and channel characterization in a compact electrical car," in *17th IEEE International Symposium on Power Line Communications and Its Applications (ISPLC), 2013*, March 2013, pp. 29–34.

[13] L. Hanzo, O. Alamri, M. El-Hajjar, and N. Wu, *Near-Capacity Multi-Functional MIMO Systems: Sphere-Packing, Iterative Detection and Cooperation*. Wiley, 2009.

[14] P. Robertson, E. Villebrun, and P. Hoeher, "A comparison of optimal and sub-optimal MAP decoding algorithms operating in the log domain," in *1995 IEEE International Conference on Communications, ICC '95 Seattle, 'Gateway to Globalization'*, vol. 2, Jun 1995, pp. 1009–1013 vol.2.

[15] T. Richardson and R. Urbanke, "The capacity of low-density parity-check codes under message-passing decoding," *IEEE Transactions on Information Theory*, vol. 47, no. 2, pp. 599–618, Feb 2001.

[16] R. Gallager, "Low-density parity-check codes," *Transactions on Information Theory*, vol. 8, no. 1, pp. 21–28, January 1962.